

# PacGDC: Label-Efficient Generalizable Depth Completion with Projection Ambiguity and Consistency

Haotian Wang<sup>1,2</sup>, Aoran Xiao<sup>2</sup>, Xiaoqin Zhang<sup>3</sup>, Meng Yang<sup>1†</sup>, Shijian Lu<sup>2†</sup>

<sup>1</sup>Xi'an Jiaotong University, <sup>2</sup>Nanyang Technological University, <sup>3</sup>Zhejiang University of Technology

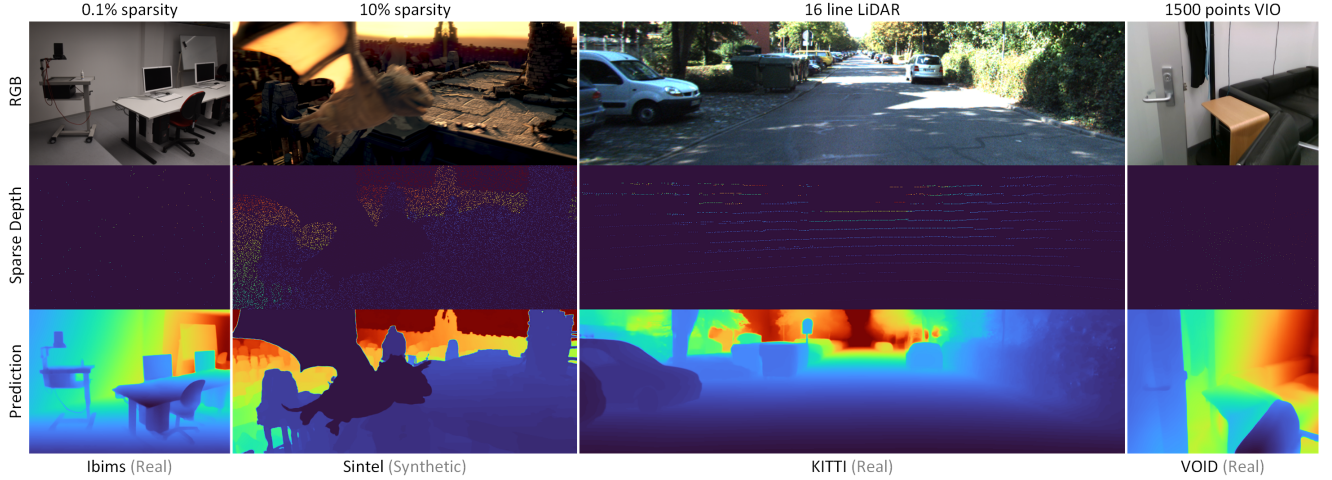


Figure 1. PacGDC generalizes effectively across unseen scenarios with a wide range of *scene semantics/scales* and *depth sparsity/patterns*. The data include real ones from Ibims [20], VOID [58], and KITTI [11], as well as synthetic ones from Sintel [3]. The sparse depths are captured from 0.1%/10% uniform sampling, 16 line vehicle LiDAR, and visual-inertial odometry (VIO) system with 1500 feature points.

## Abstract

Generalizable depth completion enables the acquisition of dense metric depth maps for unseen environments, offering robust perception capabilities for various downstream tasks. However, training such models typically requires large-scale datasets with metric depth labels, which are often labor-intensive to collect. This paper presents PacGDC, a label-efficient technique that enhances data diversity with minimal annotation effort for generalizable depth completion. PacGDC builds on novel insights into inherent ambiguities and consistencies in object shapes and positions during 2D-to-3D projection, allowing the synthesis of numerous pseudo geometries for the same visual scene. This process greatly broadens available geometries by manipulating scene scales of the corresponding depth maps. To leverage this property, we propose a new data synthesis pipeline that uses multiple depth foundation models as scale manipulators. These models robustly provide pseudo depth labels with varied scene scales, affecting both local objects and global layouts, while ensuring projection consistency

that supports generalization. To further diversify geometries, we incorporate interpolation and relocation strategies, as well as unlabeled images, extending the data coverage beyond the individual use of foundation models. Extensive experiments show that PacGDC achieves remarkable generalizability across multiple benchmarks, excelling in diverse scene semantics/scales and depth sparsity/patterns under both zero-shot and few-shot settings. Code: <https://github.com/Wang-xjtu/PacGDC>.

## 1. Introduction

Depth completion aims to infer dense metric depth maps from paired images and sparse depth measurements [7], providing accurate spatial representations that can support various downstream applications, such as robotics [4] and autonomous driving [27]. Despite its notable advancements, most existing methods suffer from poor generalization toward various new domains [50]. Recently, *generalizable depth completion* resorts to domain-agnostic models that learn from source data but enable effective deployment across various unseen downstream environments

<sup>†</sup>Corresponding author.

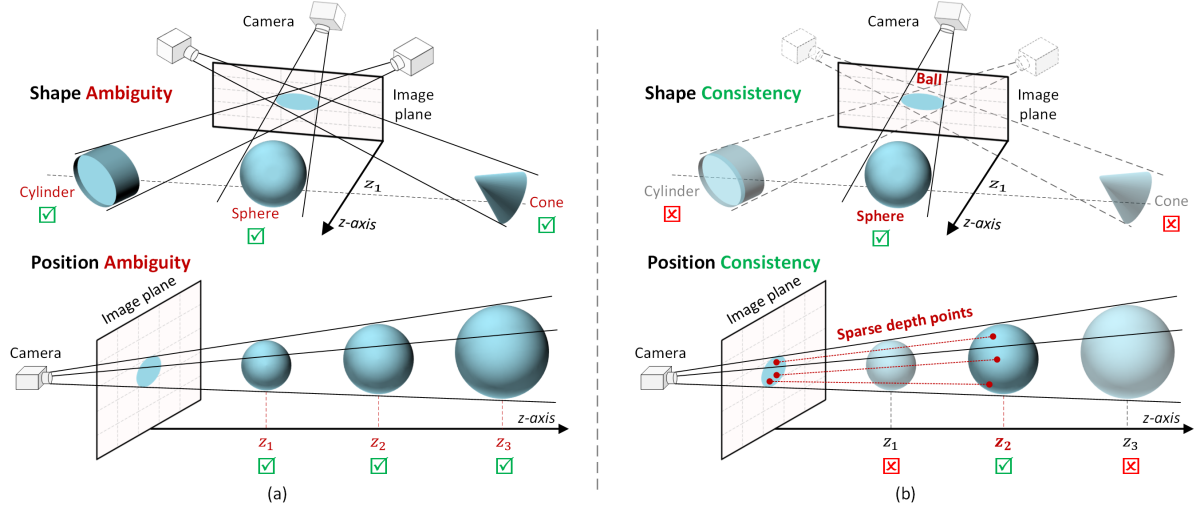


Figure 2. Illustration of the ambiguity and consistency in 2D-to-3D projections for generalizable depth completion. (a) *Ambiguity*: shape ambiguity refers that the same 2D object can correspond to different 3D shapes, while position ambiguity refers that the same 3D shape can vary in size and position. (b) *Consistency*: shape consistency denotes that the 3D shape aligns with the semantics of image input, while position consistency denotes that the 3D position is regularized by sparse depth input. The possible 3D objects are marked with  $\checkmark$ .

[51, 65]. However, the success of these studies relies heavily on large-scale dense metric depth annotations to effectively cover real-world distributions, while collecting such annotated data is often laborious and time-consuming [49].

This paper introduces PacGDC, a label-efficient technique that is designed to maximize training data coverage with minimal annotation effort for generalizable depth completion. PacGDC is grounded in 2D-to-3D *projection ambiguity*, where the same 2D image can be projected from multiple possible 3D geometric scenes [36, 72]. To leverage this ambiguity, we decompose it into two orthogonal components: *shape* and *position*, as shown in Fig. 2 (a). This decomposition reveals that each 3D geometry, defined by a depth map, can be uniquely identified by both shape and position cues. Meanwhile, these two cue types align well with the two input types in depth completion. As illustrated in Fig. 2 (b), the shape cues (e.g., “sphere”) are consistent with semantic information (e.g., “ball”) in images, while sparse depth points help regularize spatial positions. Such *consistency* mitigates ambiguity in generalizable depth completion, enabling accurate estimation of *target metric depths* across unseen scenarios, as shown in Fig. 1.

Building on these insights, this paper exploits these ambiguities to synthesize diverse pseudo geometries for the same visual scene, while maintaining consistencies among synthesized training triplets (*i.e.*, images, sparse depths, and dense depth labels). It is achieved by manipulating scene scales of the corresponding depth maps, significantly expanding available geometries without requiring additional labeled samples. Since sparse depths with consistent positions can be sampled from dense labels, as introduced in

[51, 82], our primary focus is to synthesize a large volume of pseudo dense depth labels that have consistent shapes.

Specifically, we exploit *multiple foundation models of monocular depth estimation* to synthesize qualified depth labels. These models can robustly predict dense depth maps with consistent shapes/semantics from a single image [2, 69], even across diverse unseen scenes. However, their predictions typically suffer from inaccurate scene scales, for both local objects and global layouts, due to the inherent scale ambiguity problem [56, 72]. These characteristics allow generating pseudo dense depth maps that diverge from ground-truth labels in terms of scene scales, while preserving consistency in shape cues. To further diversify geometry, we incorporate interpolation and relocation strategies, enabling additional variations beyond the predictions of any individual foundation model. With the inclusion of unlabeled data, PacGDC significantly enriches the data diversity. The full synthesis pipeline is illustrated in Fig. 4.

We conduct extensive experiments to validate the effectiveness of PacGDC in two practical applications: (1) *zero-shot testing* on seven unseen datasets with diverse sparse depth inputs, including those captured from uniform sampling, visual-inertial odometry system, and vehicle LiDAR; (2) *few-shot testing* on the KITTI dataset [11] with fewer than 1% training data. The results show that our method achieves superior generalizable depth completion.

The major contributions of this paper are threefold:

- We exploit a novel insight into 2D-to-3D projection ambiguity and consistency for generalizable depth completion, enriching data diversity without additional real labels.
- We propose a new data synthesis pipeline that manipu-

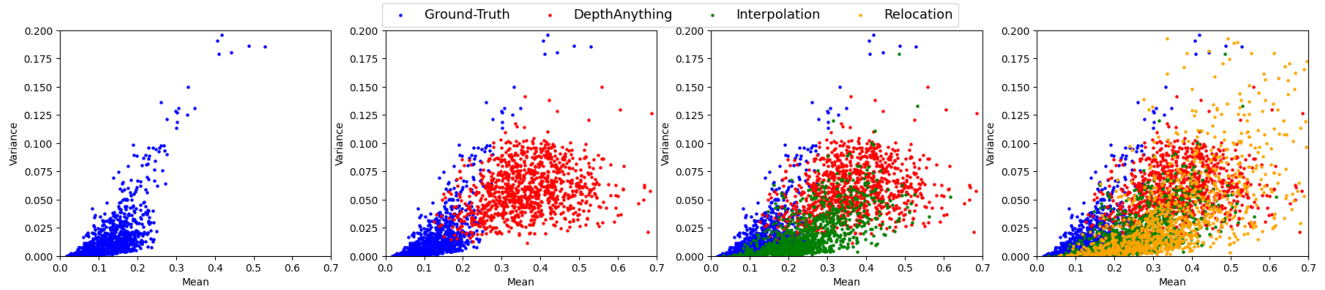


Figure 3. Data distribution of our synthesis method on 1000 samples from UnrealCV dataset [50], visualized by mean and variance. From left to right, the data diversity increases progressively with each step. Notably, this statistic is based on a single foundation model, DepthAnything [69], and a single instance of interpolation and relocation for simplicity. In the final implementation, multiple foundation models and randomized interpolation and relocation can be adopted to further enhance the data distribution.

lates local and global scene scales, enabling effective generalization to unseen domains with metric depths.

- Our approach achieves state-of-the-art performance in zero-/few-shot depth completion, validated across multiple benchmarks with different setups.

## 2. Related Work

**Depth Completion.** The success in deep learning has enabled depth completion methods to explore various dimensions including surface normal cues [34, 66, 77], semantics cues [28, 76], refinement strategies [7, 29, 45, 54], advanced backbone architectures [39, 41, 78], and sophisticated feature fusion modules [25, 55, 68, 79]. These approaches have effectively improved performance for intra-domain learning, where their training and testing data share similar scenes, such as KITTI [11] and NYUv2 [42]. However, they suffer degraded performance in unseen domains.

To address this limitation, G2-MonoDepth [50] explored a generalized framework for zero-shot scenarios. TDDC [65] incorporated pre-trained depth estimation models as a preprocessing step for enhanced image analysis. SPNet [51] investigated an important property of scale propagation within network architectures, while OMNI-DC [82] introduced multi-resolution depth guidance.

In practical applications, a limited number of training samples can be collected for cost-efficient deployment in specific environments. Conventional intra-domain methods can be directly applied in such scenarios. Recently, UniDC [30] explored few-shot depth completion using hyperbolic representation [31], while DDPMDC [35] leveraged pre-trained diffusion models to mitigate data overfitting.

**Monocular Depth Estimation.** Existing monocular depth estimation methods can be broadly categorized into three main types. First, most methods focused on predicting metric depth maps within familiar training domains [9, 74], while they struggle to generalize to unseen domains. To improve robustness, some approaches predicted relative depth

maps with normalized scales [17, 36, 37, 62, 69], which disregarded scene scales for superior generalization. Recently, the community explored predicting metric depth maps from unseen scenes by incorporating the camera focal length [2, 33, 73]. Our method manipulates the scene scales of depth maps using their dense predictions.

**Pseudo Labeling.** As a popular topic in semi-supervised learning, pseudo-labeling methods focused on leveraging unlabeled data by synthesizing pseudo labels [22]. The dominant methods aimed to improve pseudo label quality for reliable supervision, employing techniques such as threshold-based selection [18, 43, 53, 75], teacher-student frameworks [64, 80], and advanced regularization strategies [21, 43, 63]. These approaches have successfully enriched the training data of many foundational models [19, 38, 69]. In contrast, our method investigates pseudo labels upon projection ambiguity for both labeled and unlabeled data.

## 3. Method

### 3.1. Problem Definition

The training data of depth completion comprises annotated triplets, denoted  $\mathcal{T} = \{I, p, d\}$ , where  $I$  represents the input image,  $p$  is the sparse depth map captured by the depth sensors, and  $d$  is the dense depth map of ground truth. The objective is to train a model  $\mathcal{F}$ , that can predict the dense depth map  $\mathcal{F}(I, p)$  using both the input image and sparse depth map. The model is optimized by minimizing the difference between the predicted dense depth  $\mathcal{F}(I, p)$  and the ground truth  $d$ , formulated as:  $\min_{\mathcal{F}} |\mathcal{F}(I, p) - d|$ .

In the context of *generalizable* depth completion, the objective is updated to train the model  $\mathcal{F}$  on source datasets with triplets  $\mathcal{T}$ , while enabling it to effectively generalize to unseen target data, achieving strong zero-shot performance.

This paper aims to achieve superior generalizable depth completion with minimal annotation effort. We develop a label-efficient solution, PacGDC, that synthesizes pseudo triplets  $\tilde{\mathcal{T}}$  to substitute for original triplets  $\mathcal{T}$ . This signifi-

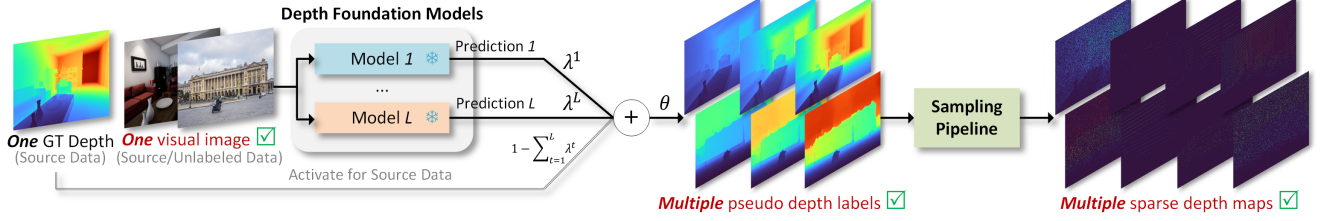


Figure 4. Overview of the proposed data synthesis pipeline, which leverages multiple depth foundation models, interpolation and relocation strategies, and unlabeled data. Sparse depth maps are then sub-sampled to form pseudo triplets (marked by ✓). This process significantly enhances data diversity through projection ambiguity while ensuring projection consistency that contributes to generalization.

cantly enhances the diversity of source data, enabling better coverage for real-world data.

Our approach addresses two main challenges:

- The theoretical process of enhancing data diversity, which we tackle by leveraging the 2D-to-3D *projection ambiguity and consistency*, as detailed in Sec. 3.2.
- The practical solution of synthesizing qualified data that contributes to generalization, for which we employ *multiple depth foundation models*, as detailed in Sec. 3.3.

### 3.2. Geometry Diversity from Projection Ambiguity and Consistency

**Projection Ambiguity.** In the pin-hole camera model [52], the 2D coordinate  $(u_i, v_i)$  in the image plane is mapped to their corresponding 3D position  $(x_i, y_i, z_i)$  at pixel  $i$  using the following projection relationship:

$$d_i P^{-1} \begin{bmatrix} u_i \\ v_i \\ 1 \end{bmatrix} = \begin{bmatrix} x_i \\ y_i \\ z_i \end{bmatrix}, \quad (1)$$

where  $P$  is the projection matrix and  $d_i$  is the depth value at pixel  $i$ . By applying a scaling factor  $\alpha_i$  to both sides of the equation, the same 2D coordinate  $(u_i, v_i)$  can correspond to a new depth value  $\hat{d}_i = \alpha_i d_i$  and a scaled 3D position  $(\alpha_i x_i, \alpha_i y_i, \alpha_i z_i)$ . This reveals that multiple 3D geometries can project onto the same 2D visual appearance  $I$ , by manipulating the scene scale of depth pixel  $d_i$ . This phenomenon is commonly referred to as *projection ambiguity* or *scale ambiguity* [36, 72].

In this paper, we decompose the projection ambiguity into two orthogonal sources, as illustrated in Fig. 2 (a):

- *Shape ambiguity* refers to that one 2D object can correspond to different 3D shapes in the same position. This implies that corresponding depth maps may share similar means but differ in variances.
- *Position ambiguity* means that the same 3D shape can vary in size and position. This suggests that their depth maps may have similar variances but varied means.

**Remark.** These ambiguities indicate that each 3D geometry can be uniquely identified by both shape and position.

**Projection Consistency.** The ambiguities suggest that predicting target 3D geometry, defined by the target depth map, requires identifying both its shape and position. In the training triplets  $\mathcal{T}$ , the input image  $I$  provides semantic cues to identify the target shape. As illustrated in Fig. 2 (b), the 2D object with semantic of “Ball” should correspond to the 3D shape of “Sphere”, rather than an unrealistic “Cone” or “Cylinder”. Meanwhile, the input sparse depth  $p$  offers sparse depth points to regularize the target position.

These consistencies of shape and position are the foundation for achieving generalizable depth completion, where *metric depths* can be effectively identified by these shape and position cues, even across diverse unseen scenarios.

**Geometry Diversity.** Building on these insights, we leverage projection ambiguity to synthesize numerous pseudo geometries for the same visual scene, while maintaining projection consistency between the input data  $I, p$  and the synthesized depth labels  $\hat{d}$ . This process can significantly enhance the geometry diversity of training data, thus achieving superior generalizability for depth completion.

We introduce the theoretical process of forming pseudo triplets  $\hat{\mathcal{T}}$  to substitute for original triplets  $\mathcal{T}$ . First, we synthesize a set of dense depth maps  $\{\hat{d}^j\}_{j=1}^N$ , where  $N$  is the number of pseudo depth labels per image. The specific synthesis method ensuring shape consistency is detailed in Sec. 3.3. Next, sparse depth maps are directly sub-sampled from each pseudo depth label, i.e.,  $\{\hat{p}^{j,k}\}_{j=1,k=1}^{N,M}$ , where  $M$  is the number of sparse depth maps per dense depth label. In this paper, we adopt the uniform sampling pipeline in [51] combined with the LiDAR&SFM patterns sampling in [82]. The sub-sampling naturally maintains consistent positions. Finally, the pseudo triplets consist of the original visual image, the pseudo depth labels, and the sampled sparse depth maps, i.e.,  $\hat{\mathcal{T}} = \{I, \{\hat{d}^j\}_{j=1}^N, \{\hat{p}^{j,k}\}_{j=1,k=1}^{N,M}\}$ . This process generates additional data combinations from the same visual images, beyond the original triplets  $\mathcal{T}$ .

### 3.3. Qualified Synthesis with Scale Manipulation

Our synthesis method aims to achieve two key objectives: (1) ensuring that the shape of the pseudo dense labels is consistent with the semantics of the input images, and (2)



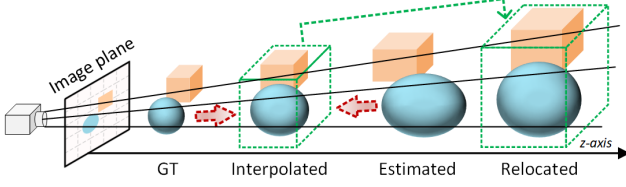


Figure 5. Illustration of basic geometry synthesis.

capturing diverse shapes and positions in the synthesized geometries. We leverage *foundation models of monocular depth estimation* to accomplish the two goals.

**Pseudo Labels from Depth Foundation Model.** Depth foundation models, such as DepthAnything [69] and DepthPro [2], are capable of robustly predicting dense depth maps with consistent semantic information from a single image, even across diverse unseen visual scenes. However, their predictions typically suffer from inaccurate scene scales due to the scale ambiguity inherent in single images [36]. For instance, the top-ranking depth estimation method [33] on the KITTI leaderboard achieves 8.24 iRMSE, significantly weaker than the top-ranking depth completion method [55] with 1.83 iRMSE. Furthermore, although many methods adopt the global affine-invariant hypothesis, their predictions exhibit scale variations not only in the global layouts but also for local objects, as discussed in [56, 72]. These characteristics enable the manipulation of local and global scene scales of pseudo depth labels to generate diverse geometries, while maintaining consistency in shape cues.

Therefore, we denote the pseudo depth labels generated by the depth foundation model  $\mathcal{R}$  from visual inputs  $I$  as  $\hat{d} = \mathcal{R}(I)$ . Unfortunately, a single  $\mathcal{R}$  only generates one type of dense prediction  $\mathcal{R}(I)$ , depending on its network architecture, training data, and training strategy. To diversify synthesized geometries, we further incorporate interpolation and relocation strategies. First, we randomly interpolate the original ground-truth depth maps  $d$  with pseudo dense labels  $\mathcal{R}(I)$ . This operation can fill the geometry coverage between them, as illustrated in Fig. 5. One limitation is that the filled coverage depends on the initial spatial positions of the two dense maps. To address this, we randomly relocate the interpolated results into new positions. The pseudo depth labels are formalized as:

$$\hat{d} = \theta(\lambda\mathcal{R}(I) + (1 - \lambda)d), \quad (2)$$

where  $\lambda$  and  $\theta$  are the random factors for interpolation and relocation, respectively. The diversity introduced by these strategies is demonstrated in Fig. 3, and their effects are also verified in the ablation study in Sec. 4.4.

**Extensions to Multiple Foundation Models and Unlabeled Images.** The basic synthesis pipeline can be extended by using multiple depth foundation models and incorporating unlabeled images. First, instead of relying on a single

Datasets	Indoor	Outdoor	Label	Size
Matterport3D [5]	✓		RGB-D	194K
HRWSI [62]	✓	✓	Stereo	20K
VKITTI [10]		✓	Synthetic	21K
UnrealCV [50]	✓	✓	Synthetic	5K
BlendedMVS [71]	✓	✓	Stereo	115K
SA1B [19] (subset)	✓	✓	<b>None</b>	390K

Table 1. The details of training datasets.

model  $\mathcal{R}$ , we update it to a set of models  $\{\mathcal{R}^t\}_{t=1}^L$ , where  $L$  denotes the number of depth foundation models. This expansion increases the variety of pseudo dense labels, yielding  $\mathcal{R}^t(I)$ . By combining these models with the interpolation and relocation strategies from Eq. (2), the pseudo depth labels are updated as follows:

$$\hat{d} = \theta \left( \sum_{t=1}^L \lambda^t \mathcal{R}^t(I) + (1 - \sum_{t=1}^L \lambda^t) d \right), \quad (3)$$

where  $\lambda^t$  is random interpolation factor for each foundation model, with the constraint  $\sum_{t=1}^L \lambda^t \leq 1$ . This paper adopts two foundation models with quite different designs as examples, including DepthAnything [69] and DepthPro [2].

As discussed in Sec. 3.2, PacGDC emphasizes assigning multiple pseudo depth labels to a single visual scene. This design shifts the model’s focus from regular *fitting dataset priors* to ours *learning geometric alignment*. It suggests that pseudo data, even without ground truth scene scale, can still contribute effectively to training generalizable depth completion models. This insight motivates us to incorporate unlabeled images  $I^u$  into our synthesis pipeline, further enriching data diversity from additional semantics and scene scales. Consequently, the set of visual images expands to  $\hat{I} = \{I, I^u\}$ . In this study, we incorporate 390K unlabeled images from SA1B dataset [19] for validation.

**Remark.** The final triplets  $\hat{\mathcal{T}}$  are constructed by three elements: visual images  $\hat{I}$ , pseudo dense labels  $\hat{d}$  generated by Eq. (3) from  $\hat{I}^1$ , and sparse depth maps  $\hat{p}$  sampled from  $\hat{d}$ .

The synthesis pipeline is illustrated in Fig. 4, which significantly enhances data diversity without requiring any additional real annotations. The ablation study of these strategies is provided in Sec. 4.4.

### 3.4. Learning from Synthesized Triplets

Learning from such large-scale, diverse, and ambiguous training data presents a challenge for existing depth completion frameworks. To effectively leverage our synthesized data, we integrate our data settings into the SPNet [51]

<sup>1</sup>Eq. (3) is available for unlabeled images by setting  $\sum_{t=1}^L \lambda^t = 1$

Methods	ETH3D		Ibims		NYUv2		DIODE		Sintel		KITTI		Mean ↓	
	RMSE	MAE	RMSE	MAE	RMSE	MAE	RMSE	MAE	RMSE	MAE	RMSE	MAE	RMSE	MAE
LRRU [54]	5226	3932	796	599	1924	1387	9014	5714	18250	13249	10783	7450	7665	5389
ImprovingDC [55]	36479	5231	1021	845	2279	1809	9451	6562	18256	13787	11705	8396	8198	6105
NLSPN [29]	2283	1367	239	116	414	210	5172	2379	43424	34221	4170	1911	9284	6701
CFormer [78]	1821	810	215	71	421	174	5176	2197	26415	21807	4400	1960	6408	4503
G2MD [50]	1420	691	196	58	382	150	5026	2114	3612	917	3690	1607	2387	923
SPNet [51]	1544	569	177	47	399	154	5070	2078	3312	659	3124	1240	2271	791
OMNI-DC [82]	929	<b>420</b>	<u>165</u>	<u>46</u>	<b>357</b>	<b>139</b>	<u>4848</u>	<u>2076</u>	7733	3989	<u>3050</u>	<u>1191</u>	2847	1310
<b>Ours</b>	<b>907</b>	<u>454</u>	<b>160</b>	<b>46</b>	<u>376</u>	<u>147</u>	<b>4721</b>	<b>1984</b>	<b>2961</b>	<b>580</b>	<b>2673</b>	<b>1172</b>	<b>1966</b>	<b>731</b>

Table 2. **Zero-shot depth completion** on the six datasets with sparse depth maps obtained by uniformly sampling 10%/1%/0.1% valid pixels. The **bold** indicates the best result, and the underline indicates the second-best result.

Methods	VOID-1500		VOID-500		VOID-150		KITTI-64L		KITTI-16L		KITTI-4L		Mean ↓	
	RMSE	MAE	RMSE	MAE	RMSE	MAE	RMSE	MAE	RMSE	MAE	RMSE	MAE	RMSE	MAE
LRRU [54]	835	530	937	637	1000	685	2124	742	4968	2943	12658	9466	3753	2501
ImprovingDC [55]	950	595	1160	850	1251	949	2200	1118	4281	2325	11421	8044	3544	2313
NLSPN [29]	431	156	484	192	571	247	1627	501	2174	711	4133	1690	1570	583
CFormer [78]	426	144	460	170	522	208	1513	359	2221	601	4768	1835	1652	553
G2MD [50]	383	117	417	141	484	181	1570	352	2138	572	3941	1648	1489	502
SPNet [51]	<u>353</u>	<u>104</u>	<u>375</u>	<u>119</u>	<u>430</u>	<u>151</u>	1523	<u>331</u>	2108	537	3268	1148	1343	398
OMNI-DC [82]	391	121	422	143	478	177	<b>1191</b>	<b>270</b>	<b>1682</b>	<b>441</b>	2981	997	1191	358
<b>Ours</b>	<b>348</b>	<b>102</b>	<b>363</b>	<b>114</b>	<b>409</b>	<b>141</b>	<u>1375</u>	337	<u>1702</u>	<u>460</u>	<b>2685</b>	<b>896</b>	<b>1147</b>	<b>342</b>

Table 3. **Zero-shot depth completion** on VOID dataset with 1500/500/150 sparsity levels from visual-inertial odometry system, and KITTI dataset with 64/16/4 beam lines from vehicle LiDAR.

framework, known for its efficiency and strong generalization ability. The source training datasets, detailed in Tab. 1, include 355K labeled samples and 390K unlabeled samples. **Computational Cost Analysis.** Since our work focuses on training data diversity, it does not introduce any additional computational cost during inference. This ensures that our model fully retains the efficient inference of SPNet, whose “Tiny” model achieves 126.6 image/s on a single 3090 GPU at 320×320 resolution. In comparison, competing methods such as G2-MonoDepth [50] and OMNI-DC [2] achieve only 69.5% and 8.4% of SPNet’s speed, respectively.

The computational cost is primarily introduced during training. Our method consists of four main components: depth foundation models, unlabeled images, interpolation, and relocation. The latter two introduce only minimal additional multiplication and addition operations. For depth foundation models, their predictions can be precomputed and loaded on demand. Therefore, the primary additional cost derives from unlabeled images, resulting in an additional 390K/355K computations in our implementation.

## 4. Experiment

Our experiments consider two practical applications: *zero-shot depth completion* in Sec. 4.2 and *few-shot depth completion* in Sec. 4.3. Additional experimental results are included in the supplementary materials.

### 4.1. Settings

**Evaluation Protocol.** *Zero-shot depth completion:* Following zero-shot depth estimation [69], we impose no restrictions on the model training, evaluating only released models on the same test setups. The test datasets include two types: (1) sparse depth maps obtained by uniformly sampling 10%/1%/0.1% of valid pixels from the ETH3D [40], Ibims [20], NYUv2 [42], DIODE [46], Sintel [3], and KITTI [11] datasets, as used in [50, 51]; (2) sparse depth points captured by visual-inertial odometry system with 1500/500/150 sparsity levels on VOID [58] dataset, and by vehicle LiDAR with 64/16/4 beam lines on KITTI dataset. *Few-shot depth completion:* All models are trained on sequentially selected subsets of 1, 10, 100, and 1000 samples from the KITTI training set (*i.e.*, 86K samples), and evaluated on its validation set with 1000 test samples.

**Implementation Details.** *Zero-shot depth completion:* We adopt the “Large” model of SPNet for the best performance, while sacrificing 47% inference speed. The model is trained using the AdamW optimizer with batch size 192, running on six 3090 GPUs. The initial learning rate is 0.0002 with cosine learning rate decay using 100 epochs. *Few-shot depth completion:* Our models are initialized by pre-trained weights from the zero-shot phase. We adopt 1/10 initial learning rate for this fine-tuning. The batch sizes are set to {1, 1, 4, 4} when using {1, 10, 100, 1000} training samples.

Shot	Methods	RMSE ↓	MAE ↓	iRMSE ↓	iMAE ↓
1	LRRU [54]	2138	679	95.69	2.94
	ImprovingDC [55]	1358	337	4.68	1.43
	SparseDC [25]	1757	636	8.30	3.65
	UniDC [30]	1684	522	-	-
	<b>Ours</b>	<b>1078</b>	<b>250</b>	<b>2.90</b>	<b>0.98</b>
10	LRRU [54]	1337	342	5.54	1.38
	ImprovingDC [55]	1316	315	4.13	1.26
	SparseDC [25]	1438	380	10.22	1.86
	UniDC [30]	1385	407	-	-
	<b>Ours</b>	<b>969</b>	<b>238</b>	<b>2.70</b>	<b>0.96</b>
100	LRRU [54]	1261	295	4.02	1.17
	ImprovingDC [55]	1241	304	4.01	1.27
	SparseDC [25]	1203	325	4.42	1.48
	UniDC [30]	1224	339	-	-
	<b>Ours</b>	<b>911</b>	<b>229</b>	<b>2.54</b>	<b>0.96</b>
1000	LRRU [54]	1105	266	3.34	1.09
	ImprovingDC [55]	1121	279	3.79	1.15
	SparseDC [25]	1049	263	3.57	1.14
	<b>Ours</b>	<b>830</b>	<b>220</b>	<b>2.28</b>	<b>0.91</b>

Table 4. **Few-shot depth completion** on KITTI with 64 line LiDAR using 1, 10, 100, and 1000 training samples.

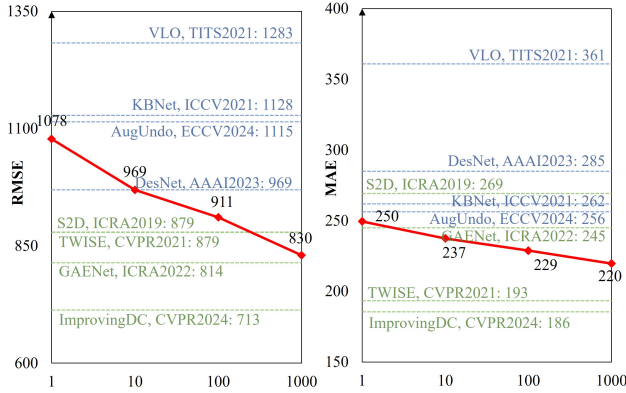


Figure 6. “**Few-shot vs full-shot**” on KITTI with 64 line LiDAR. The horizontal axis denotes that our models use 1, 10, 100, and 1000 training samples, while the baselines use 86K samples. The **self-supervised** baselines include VLO [44], KBNet [57], AugUndo [61], and DesNet [67]. The **supervised** baselines include S2D [26], TWISE [16], GAENet [6], and ImprovingDC [55].

**Baseline Details.** *Zero-shot depth completion:* The baselines include several generalizable depth completion methods: G2-MonoDepth (G2MD) [50], OMNI-DC [82], and SPNet [51], as well as fully supervised methods: NLSPN [29], CFormer [78], LRRU [54], and ImprovingDC [55]. To ensure zero-shot testing, the fully supervised methods are retrained on large-scale datasets provided by SPNet. *Few-shot depth completion:* We retrained recent methods, LRRU [54], ImprovingDC [55], and SparseDC [25] in the same few-shot setting for direct comparison. The official results of UniDC [30] are listed for reference. To highlight our

Shot	Methods	RMSE ↓	MAE ↓	iRMSE ↓	iMAE ↓
1	LRRU [54]	5558	3708	259.59	23.60
	ImprovingDC [55]	3322	1473	12.69	7.22
	SparseDC [25]	5950	3997	12598.67	250.22
	<b>Ours</b>	<b>1662</b>	<b>455</b>	<b>3.54</b>	<b>1.42</b>
10	LRRU [54]	3206	1329	12.30	5.56
	ImprovingDC [55]	3092	1350	13.06	6.20
	SparseDC [25]	3507	1659	50.56	9.61
	<b>Ours</b>	<b>1524</b>	<b>426</b>	<b>3.32</b>	<b>1.37</b>
100	LRRU [54]	2646	1014	14.14	4.37
	ImprovingDC [55]	2642	1043	10.07	4.55
	SparseDC [25]	2235	798	19.30	3.47
	<b>Ours</b>	<b>1425</b>	<b>339</b>	<b>3.07</b>	<b>1.29</b>
1000	LRRU [54]	2092	713	6.21	2.79
	ImprovingDC [55]	2259	843	7.82	3.67
	SparseDC [25]	1863	606	5.79	2.36
	<b>Ours</b>	<b>1297</b>	<b>371</b>	<b>2.82</b>	<b>1.22</b>

Table 5. **Few-shot depth completion** on KITTI with 64/32/16/8/4 lines LiDAR using 1, 10, 100, and 1000 training samples.

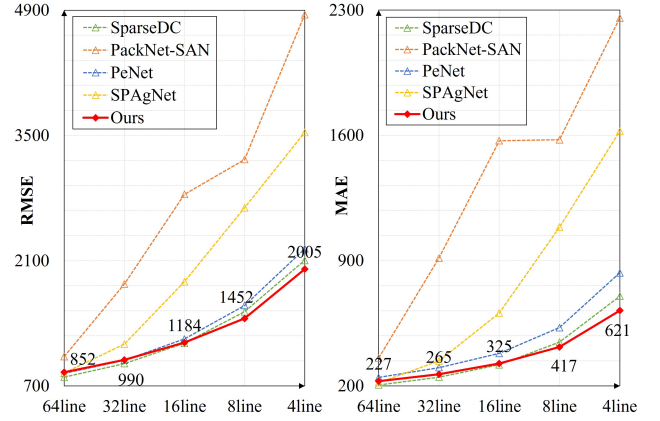


Figure 7. “**Few-shot vs full-shot**” on KITTI with 64/32/16/8/4 lines LiDAR. Our model is trained with 1000 samples, while the baselines use 86K samples including SparseDC [25], PackNet-SAN [13], PeNet [15], and SPAGNet [8].

model, we further evaluate it, using less than 1000 samples, against full-shot baselines, trained with 86k samples. Their results are directly taken from the original papers.

**Metric Details.** We use standard evaluation metrics including root mean square error (RMSE), mean absolute error (MAE), root mean square error of the inverse depth (iRMSE), and mean absolute error of the inverse depth (iMAE). All results are reported in *millimeters (mm)*.

## 4.2. Zero-Shot Depth Completion

In this section, we show model capability across zero-shot environments, which is unobserved during training.

**Uniformly Sampled Depths.** We begin evaluation on sparse depth maps with uniformly sampled valid pixels at 10%/1%/0.1% sparsity levels, across six unseen datasets.

Framework	Speed (image/s)	Basic Synthesis Method			Extensions		RMSE ↓	MAE ↓
		<i>DepthAnything</i> [69]	<i>P(Interpolation)</i>	<i>Relocation</i>	<i>DepthPro</i> [2]	<i>SA1B (subset)</i> [19]		
SPNet [51] ( <i>Tiny</i> )	126.6	✓	0.0				2484	990
		✓	0.25				2463	956
		✓	0.5				2380	912
		✓	1.0				2344	889
		✓	1.0	✓			2330	889
		✓	1.0	✓	✓		2277	857
		✓	1.0	✓	✓		2241	854
		✓	1.0	✓	✓	✓	<b>2143</b>	<b>792</b>
G2MD [50]	88.0	✓	1.0	✓	✓	✓	2669	1101
							<b>2192</b>	<b>817</b>

Table 6. **Ablation study** of our synthesis method based on two types of generalizable depth completion frameworks.

The average results are summarized in Tab. 2, in which our model performs the best in most scenarios, with the lowest RMSE 1966 mm and MAE 731 mm on average.

**Sensor Captured Depths.** Next, we evaluate sparse depth points captured by physical sensors on two unseen datasets: VOID [58] dataset with 1500/500/150 sparsity levels, and KITTI [11] dataset with 64/16/4 lines LiDAR. Tab. 3 shows that our model still outperforms all baseline models with the lowest RMSE 1147 mm and MAE 342 mm on average.

**Visual Results.** Fig. 1 has presented several visual results. Additional results can be found in supplementary material.

### 4.3. Few-Shot Depth Completion

In this section, we fine-tune our model in the specific environment to compete for intro-domain learning methods, on KITTI dataset with 1, 10, 100, and 1000 samples.

**64 line LiDAR Depths.** We train and test all models using 64 line LiDAR under the few-shot setting. Tab. 4 shows that our model significantly outperforms these baselines designed for intro-domain learning. We attribute this strong performance to powerful pre-trained weights by our synthesis method. These weights provide an excellent starting point to regularize this few-shot learning.

Additionally, we compare our few-shot model against baselines trained on the full 86K samples. As shown in Fig. 6, our model achieves competitive results, outperforming all self-supervised baselines in MAE with just a single annotated sample. When using 1000 training samples, our model even outperforms supervised baselines such as S2D and TWISE in RMSE, as well as S2D and GAENet in MAE.

**64/32/16/8/4 lines LiDAR Depths.** We also train all models on randomly sampled 64/32/16/8/4 lines LiDAR, and test them in each beam line. Tab. 5 shows the average results across these beam lines, and our models also outperform baseline methods. As shown in Fig. 7, our few-shot model, trained with just 1000 samples, achieves competitive results of full-shot baselines. Notably, our model achieves the best RMSE and MAE on 8/4 lines LiDAR data.

### 4.4. Ablation Study

In this section, we verify each component of our synthesis method. Due to computational constraints, we adopt the “Tiny” model of SPNet using 25% of the full data.

**Basic Synthesis Method.** Our synthesis method consists of three components to implement the basic approach outlined in Eq. (2): the incorporation of a depth foundation model (*i.e.*, *DepthAnything* [69]), interpolation operation (*i.e.*,  $P(\text{Interpolation}) = 1.0$ ), and relocation operation. As shown in Tab. 6, each of these steps progressively improves prediction quality by enhancing the geometry diversity.

**Extension Examples.** The basic synthesis method can be extended by integrating multiple depth foundation models and unlabeled data, as discussed in Sec. 3.3. For verification, we further incorporate an depth foundation model, *DepthPro* [2], and 390K unlabeled images from SA1B [19]. The effectiveness of these extensions is shown in Tab. 6.

**Interpolated vs Original Labels.** To further show the effectiveness of interpolated labels, we adjust the probability of using interpolated labels (*i.e.*,  $P(\text{Interpolation})$ ) from 0.0 to 1.0. The remaining probability is used for randomly selecting original dense depth maps, including ground-truth depth maps and dense predictions from *DepthAnything*. As shown in Tab. 6, when using fully interpolated depth labels (*i.e.*,  $P(\text{Interpolation}) = 1.0$ ), the model achieves the best performance due to maximized data diversity.

## 5. Conclusion

In this paper, we propose a label-efficient method, PacGDC, to expand training data coverage with minimal annotation effort for generalizable depth completion. This is achieved by a data synthesis pipeline based on the 2D-to-3D projection ambiguities and consistencies. This pipeline includes multiple depth foundation models, interpolation and relocation strategies, and unlabeled data. Extensive experiments demonstrate that PacGDC achieves superior generalizable depth completion in both zero-shot and few-shot settings.



## Acknowledgment

This work was supported in part by the National Natural Science Foundation of China (NSFC) under Grants 62088102 and 62373298, and by the Singapore Ministry of Education (MOE) Tier-2 Grant MOE-T2EP20123-0003.

## References

- [1] Luca Bartolomei, Matteo Poggi, Andrea Conti, Fabio Tosi, and Stefano Mattoccia. Revisiting depth completion from a stereo matching perspective for cross-domain generalization. In *2024 International Conference on 3D Vision (3DV)*, pages 1360–1370. IEEE, 2024. 1
- [2] Aleksei Bochkovskii, Amaël Delaunoy, Hugo Germain, Marcel Santos, Yichao Zhou, Stephan R Richter, and Vladlen Koltun. Depth pro: Sharp monocular metric depth in less than a second. *arXiv preprint arXiv:2410.02073*, 2024. 2, 3, 5, 6, 8
- [3] Daniel J Butler, Jonas Wulff, Garrett B Stanley, and Michael J Black. A naturalistic open source movie for optical flow evaluation. In *European Conference on Computer Vision*, pages 611–625. Springer, 2012. 1, 6
- [4] Carlos Campos, Richard Elvira, Juan J Gómez Rodríguez, José MM Montiel, and Juan D Tardós. Orb-slam3: An accurate open-source library for visual, visual-inertial, and multi-map slam. *IEEE Transactions on Robotics*, 37(6):1874–1890, 2021. 1
- [5] Angel Chang, Angela Dai, Thomas Funkhouser, Maciej Halber, Matthias Niessner, Manolis Savva, Shuran Song, Andy Zeng, and Yinda Zhang. Matterport3d: Learning from rgb-d data in indoor environments. *arXiv preprint arXiv:1709.06158*, 2017. 5
- [6] Hu Chen, Hongyu Yang, Yi Zhang, et al. Depth completion using geometry-aware embedding. In *2022 International Conference on Robotics and Automation (ICRA)*, pages 8680–8686. IEEE, 2022. 7
- [7] Xinjing Cheng, Peng Wang, and Ruigang Yang. Learning depth with convolutional spatial propagation network. *IEEE transactions on pattern analysis and machine intelligence*, 42(10):2361–2379, 2019. 1, 3
- [8] Andrea Conti, Matteo Poggi, and Stefano Mattoccia. Sparsity agnostic depth completion. In *Proceedings of the IEEE/CVF winter conference on applications of computer vision*, pages 5871–5880, 2023. 7
- [9] Huan Fu, Mingming Gong, Chaohui Wang, Kayhan Batmanghelich, and Dacheng Tao. Deep ordinal regression network for monocular depth estimation. In *Proceedings of the IEEE conference on computer vision and pattern recognition*, pages 2002–2011, 2018. 3
- [10] Adrien Gaidon, Qiao Wang, Yohann Cabon, and Eleonora Vig. Virtual worlds as proxy for multi-object tracking analysis. In *Proceedings of the IEEE conference on computer vision and pattern recognition*, pages 4340–4349, 2016. 5
- [11] Andreas Geiger, Philip Lenz, and Raquel Urtasun. Are we ready for autonomous driving? the kitti vision benchmark suite. In *Proceedings of the IEEE/CVF Conference on Computer Vision and Pattern Recognition*, pages 3354–3361. IEEE, 2012. 1, 2, 3, 6, 8
- [12] Vitor Guizilini, Rares Ambrus, Sudeep Pillai, Allan Rantos, and Adrien Gaidon. 3d packing for self-supervised monocular depth estimation. In *Proceedings of the IEEE/CVF conference on computer vision and pattern recognition*, pages 2485–2494, 2020. 1
- [13] Vitor Guizilini, Rares Ambrus, Wolfram Burgard, and Adrien Gaidon. Sparse auxiliary networks for unified monocular depth prediction and completion. In *Proceedings of the IEEE/CVF conference on computer vision and pattern recognition*, pages 11078–11088, 2021. 7
- [14] Xiankang He, Dongyan Guo, Hongji Li, Ruibo Li, Ying Cui, and Chi Zhang. Distill any depth: Distillation creates a stronger monocular depth estimator. *Proceedings of the IEEE/CVF Conference on Computer Vision and Pattern Recognition*, 2025. 2
- [15] Mu Hu, Shuling Wang, Bin Li, Shiyu Ning, Li Fan, and Xiaojin Gong. Penet: Towards precise and efficient image guided depth completion. In *2021 IEEE International Conference on Robotics and Automation (ICRA)*, pages 13656–13662. IEEE, 2021. 7
- [16] Saif Imran, Xiaoming Liu, and Daniel Morris. Depth completion with twin surface extrapolation at occlusion boundaries. In *Proceedings of the IEEE/CVF Conference on Computer Vision and Pattern Recognition*, pages 2583–2592, 2021. 7
- [17] Bingxin Ke, Anton Obukhov, Shengyu Huang, Nando Metzger, Rodrigo Caye Daudt, and Konrad Schindler. Repurposing diffusion-based image generators for monocular depth estimation. In *Proceedings of the IEEE/CVF Conference on Computer Vision and Pattern Recognition*, pages 9492–9502, 2024. 3
- [18] Jiwon Kim, Youngjo Min, Daehwan Kim, Gyuseong Lee, Junyoung Seo, Kwangrok Ryoo, and Seungryong Kim. Comatch: Semi-supervised learning with confidence-guided consistency regularization. In *European Conference on Computer Vision*, pages 674–690. Springer, 2022. 3
- [19] Alexander Kirillov, Eric Mintun, Nikhila Ravi, Hanzi Mao, Chloe Rolland, Laura Gustafson, Tete Xiao, Spencer Whitehead, Alexander C Berg, Wan-Yen Lo, et al. Segment anything. In *Proceedings of the IEEE/CVF International Conference on Computer Vision*, pages 4015–4026, 2023. 3, 5, 8
- [20] Tobias Koch, Lukas Liebel, Friedrich Fraundorfer, and Marco Korner. Evaluation of cnn-based single-image depth estimation methods. In *Proceedings of the European Conference on Computer Vision (ECCV) Workshops*, pages 0–0, 2018. 1, 6
- [21] Junnan Li, Caiming Xiong, and Steven CH Hoi. Comatch: Semi-supervised learning with contrastive graph regularization. In *Proceedings of the IEEE/CVF international conference on computer vision*, pages 9475–9484, 2021. 3
- [22] Siyuan Li, Weiyang Jin, Zedong Wang, Fang Wu, Zicheng Liu, Cheng Tan, and Stan Z Li. Semireward: A general reward model for semi-supervised learning. *arXiv preprint arXiv:2310.03013*, 2023. 3

- [23] Yingping Liang, Yutao Hu, Wenqi Shao, and Ying Fu. Distilling monocular foundation model for fine-grained depth completion. In *Proceedings of the Computer Vision and Pattern Recognition Conference*, pages 22254–22265, 2025. 1
- [24] Ze Liu, Yutong Lin, Yue Cao, Han Hu, Yixuan Wei, Zheng Zhang, Stephen Lin, and Baining Guo. Swin transformer: Hierarchical vision transformer using shifted windows. In *Proceedings of the IEEE/CVF international conference on computer vision*, pages 10012–10022, 2021. 1
- [25] Chen Long, Wenxiao Zhang, Zhe Chen, Haiping Wang, Yuan Liu, Peiling Tong, Zhen Cao, Zhen Dong, and Bisheng Yang. Sparsedc: Depth completion from sparse and non-uniform inputs. *Information Fusion*, 110:102470, 2024. 3, 7
- [26] Fangchang Ma, Guilherme Venturelli Cavalheiro, and Sertac Karaman. Self-supervised sparse-to-dense: Self-supervised depth completion from lidar and monocular camera. In *2019 International Conference on Robotics and Automation (ICRA)*, pages 3288–3295. IEEE, 2019. 7
- [27] Ruihang Miao, Weizhou Liu, Mingrui Chen, Zheng Gong, Weixin Xu, Chen Hu, and Shuchang Zhou. Occdepth: A depth-aware method for 3d semantic scene completion. *arXiv preprint arXiv:2302.13540*, 2023. 1
- [28] Danish Nazir, Alain Pagani, Marcus Liwicki, Didier Stricker, and Muhammad Zeshan Afzal. Semattnet: Toward attention-based semantic aware guided depth completion. *IEEE Access*, 10:120781–120791, 2022. 3
- [29] Jinsun Park, Kyungdon Joo, Zhe Hu, Chi-Kuei Liu, and In So Kweon. Non-local spatial propagation network for depth completion. In *European Conference on Computer Vision*, pages 120–136. Springer, 2020. 3, 6, 7, 1
- [30] Jin-Hwi Park and Hae-Gon Jeon. A simple yet universal framework for depth completion. In *The Thirty-eighth Annual Conference on Neural Information Processing Systems*, 2024. 3, 7, 2
- [31] Jin-Hwi Park, Jaesung Choe, Inhwan Bae, and Hae-Gon Jeon. Learning affinity with hyperbolic representation for spatial propagation. In *Proceedings of the International Conference on Machine Learning (ICML)*, 2023. 3
- [32] Jin-Hwi Park, Chanhwi Jeong, Junoh Lee, and Hae-Gon Jeon. Depth prompting for sensor-agnostic depth estimation. In *Proceedings of the IEEE/CVF Conference on Computer Vision and Pattern Recognition*, pages 9859–9869, 2024. 2
- [33] Luigi Piccinelli, Yung-Hsu Yang, Christos Sakaridis, Mattia Segu, Siyuan Li, Luc Van Gool, and Fisher Yu. Unidepth: Universal monocular metric depth estimation. In *Proceedings of the IEEE/CVF Conference on Computer Vision and Pattern Recognition*, pages 10106–10116, 2024. 3, 5
- [34] Jiaxiong Qiu, Zhaopeng Cui, Yinda Zhang, Xingdi Zhang, Shuaicheng Liu, Bing Zeng, and Marc Pollefeys. DeepLidar: Deep surface normal guided depth prediction for outdoor scene from sparse lidar data and single color image. In *Proceedings of the IEEE/CVF Conference on Computer Vision and Pattern Recognition*, pages 3313–3322, 2019. 3
- [35] Weihang Ran, Wei Yuan, and Ryosuke Shibasaki. Few-shot depth completion using denoising diffusion probabilistic model. In *Proceedings of the IEEE/CVF Conference on Computer Vision and Pattern Recognition*, pages 6559–6567, 2023. 3, 2
- [36] René Ranftl, Katrin Lasinger, David Hafner, Konrad Schindler, and Vladlen Koltun. Towards robust monocular depth estimation: Mixing datasets for zero-shot cross-dataset transfer. *IEEE Transactions on Pattern Analysis and Machine Intelligence*, 44(3):1623–1637, 2020. 2, 3, 4, 5
- [37] René Ranftl, Alexey Bochkovskiy, and Vladlen Koltun. Vision transformers for dense prediction. In *Proceedings of the IEEE/CVF international conference on computer vision*, pages 12179–12188, 2021. 3
- [38] Nikhila Ravi, Valentin Gabeur, Yuan-Ting Hu, Ronghang Hu, Chaitanya Ryali, Tengyu Ma, Haitham Khedr, Roman Rädle, Chloe Rolland, Laura Gustafson, et al. Sam 2: Segment anything in images and videos. *arXiv preprint arXiv:2408.00714*, 2024. 3
- [39] Kyeongha Rho, Jinsung Ha, and Youngjung Kim. Guideformer: Transformers for image guided depth completion. In *Proceedings of the IEEE/CVF Conference on Computer Vision and Pattern Recognition*, pages 6250–6259, 2022. 3
- [40] Thomas Schops, Johannes L Schonberger, Silvano Galliani, Torsten Sattler, Konrad Schindler, Marc Pollefeys, and Andreas Geiger. A multi-view stereo benchmark with high-resolution images and multi-camera videos. In *Proceedings of the IEEE conference on computer vision and pattern recognition*, pages 3260–3269, 2017. 6, 1
- [41] Shuwei Shao, Ran Li, Zhongcai Pei, Zhong Liu, Weihai Chen, Wentao Zhu, Xingming Wu, and Baochang Zhang. Towards comprehensive monocular depth estimation: Multiple heads are better than one. *IEEE Transactions on Multimedia*, 25:7660–7671, 2022. 3
- [42] Nathan Silberman, Derek Hoiem, Pushmeet Kohli, and Rob Fergus. Indoor segmentation and support inference from rgbd images. In *European Conference on Computer Vision*, pages 746–760. Springer, 2012. 3, 6, 1
- [43] Kihyuk Sohn, David Berthelot, Nicholas Carlini, Zizhao Zhang, Han Zhang, Colin A Raffel, Ekin Dogus Cubuk, Alexey Kurakin, and Chun-Liang Li. Fixmatch: Simplifying semi-supervised learning with consistency and confidence. *Advances in Neural Information Processing Systems*, 33:596–608, 2020. 3
- [44] Zhenbo Song, Jianfeng Lu, Yazhou Yao, and Jian Zhang. Self-supervised depth completion from direct visual-lidar odometry in autonomous driving. *IEEE Transactions on Intelligent Transportation Systems*, 23(8):11654–11665, 2021. 7
- [45] Jie Tang, Fei-Peng Tian, Boshi An, Jian Li, and Ping Tan. Bilateral propagation network for depth completion. In *Proceedings of the IEEE/CVF Conference on Computer Vision and Pattern Recognition*, pages 9763–9772, 2024. 3, 1
- [46] Igor Vasiljevic, Nick Kolkin, Shanyi Zhang, Ruotian Luo, Haochen Wang, Falcon Z Dai, Andrea F Daniele, Mohammadreza Mostajabi, Steven Basart, Matthew R Walter, et al. Diode: A dense indoor and outdoor depth dataset. *arXiv preprint arXiv:1908.00463*, 2019. 6, 1
- [47] Massimiliano Viola, Kevin Qu, Nando Metzger, Bingxin Ke, Alexander Becker, Konrad Schindler, and Anton Obukhov. Marigold-dc: Zero-shot monocular depth completion with guided diffusion. *arXiv preprint arXiv:2412.13389*, 2024. 1

- [48] Haotian Wang, Meng Yang, Xuguang Lan, Ce Zhu, and Nanning Zheng. Depth map recovery based on a unified depth boundary distortion model. *IEEE transactions on image processing*, 31:7020–7035, 2022. 1
- [49] Haotian Wang, Meng Yang, Ce Zhu, and Nanning Zheng. Rgb-guided depth map recovery by two-stage coarse-to-fine dense crf models. *IEEE Transactions on Image Processing*, 32:1315–1328, 2023. 2, 1
- [50] Haotian Wang, Meng Yang, and Nanning Zheng. G2-monodepth: A general framework of generalized depth inference from monocular rgb+ x data. *IEEE Transactions on Pattern Analysis and Machine Intelligence*, 46(5):3753–3771, 2024. 1, 3, 5, 6, 7, 8
- [51] Haotian Wang, Meng Yang, Xinhui Zheng, and Gang Hua. Scale propagation network for generalizable depth completion. *IEEE Transactions on Pattern Analysis and Machine Intelligence*, 47(3):1908–1922, 2025. 2, 3, 4, 5, 6, 7, 8, 1
- [52] Shuzhe Wang, Vincent Leroy, Yohann Cabon, Boris Chidlovskii, and Jerome Revaud. Dust3r: Geometric 3d vision made easy. In *Proceedings of the IEEE/CVF Conference on Computer Vision and Pattern Recognition*, pages 20697–20709, 2024. 4
- [53] Yidong Wang, Hao Chen, Qiang Heng, Wenxin Hou, Yue Fan, Zhen Wu, Jindong Wang, Marios Savvides, Takahiro Shinozaki, Bhiksha Raj, et al. Freematch: Self-adaptive thresholding for semi-supervised learning. *arXiv preprint arXiv:2205.07246*, 2022. 3
- [54] Yufei Wang, Bo Li, Ge Zhang, Qi Liu, Tao Gao, and Yuchao Dai. Lrru: Long-short range recurrent updating networks for depth completion. In *Proceedings of the IEEE/CVF International Conference on Computer Vision*, pages 9422–9432, 2023. 3, 6, 7, 1
- [55] Yufei Wang, Ge Zhang, Shaoqian Wang, Bo Li, Qi Liu, Le Hui, and Yuchao Dai. Improving depth completion via depth feature upsampling. In *Proceedings of the IEEE/CVF Conference on Computer Vision and Pattern Recognition*, pages 21104–21113, 2024. 3, 5, 6, 7, 1
- [56] Diana Wofk, René Ranftl, Matthias Müller, and Vladlen Koltun. Monocular visual-inertial depth estimation. In *2023 IEEE International Conference on Robotics and Automation (ICRA)*, pages 6095–6101. IEEE, 2023. 2, 5
- [57] Alex Wong and Stefano Soatto. Unsupervised depth completion with calibrated backprojection layers. In *Proceedings of the IEEE/CVF International Conference on Computer Vision*, pages 12747–12756, 2021. 7
- [58] Alex Wong, Xiaohan Fei, Stephanie Tsuei, and Stefano Soatto. Unsupervised depth completion from visual inertial odometry. *IEEE Robotics and Automation Letters*, 5(2):1899–1906, 2020. 1, 6, 8
- [59] Sanghyun Woo, Shoubhik Debnath, Ronghang Hu, Xinlei Chen, Zhuang Liu, In So Kweon, and Saining Xie. Convnext v2: Co-designing and scaling convnets with masked autoencoders. In *Proceedings of the IEEE/CVF Conference on Computer Vision and Pattern Recognition*, pages 16133–16142, 2023. 1
- [60] Shuang Wu, Guanrui Wang, Pei Tang, Feng Chen, and Luping Shi. Convolution with even-sized kernels and symmetric padding. *Advances in Neural Information Processing Systems*, 32, 2019. 1
- [61] Yangchao Wu, Tian Yu Liu, Hyoungseob Park, Stefano Soatto, Dong Lao, and Alex Wong. Augundo: Scaling up augmentations for monocular depth completion and estimation. In *European Conference on Computer Vision*, 2024. 7
- [62] Ke Xian, Jianming Zhang, Oliver Wang, Long Mai, Zhe Lin, and Zhiguo Cao. Structure-guided ranking loss for single image depth prediction. In *Proceedings of the IEEE/CVF Conference on Computer Vision and Pattern Recognition*, pages 611–620, 2020. 3, 5
- [63] Qizhe Xie, Zihang Dai, Eduard Hovy, Thang Luong, and Quoc Le. Unsupervised data augmentation for consistency training. *Advances in Neural Information Processing Systems*, 33:6256–6268, 2020. 3
- [64] Qizhe Xie, Minh-Thang Luong, Eduard Hovy, and Quoc V Le. Self-training with noisy student improves imagenet classification. In *Proceedings of the IEEE/CVF Conference on Computer Vision and Pattern Recognition*, pages 10687–10698, 2020. 3
- [65] Guangkai Xu, Wei Yin, Jianming Zhang, Oliver Wang, Simon Niklaus, Simon Chen, and Jia-Wang Bian. Towards domain-agnostic depth completion. *Machine Intelligence Research*, pages 1–18, 2024. 2, 3
- [66] Yan Xu, Xinge Zhu, Jianping Shi, Guofeng Zhang, Hujun Bao, and Hongsheng Li. Depth completion from sparse lidar data with depth-normal constraints. In *Proceedings of the IEEE/CVF International Conference on Computer Vision*, pages 2811–2820, 2019. 3
- [67] Zhiqiang Yan, Kun Wang, Xiang Li, Zhenyu Zhang, Jun Li, and Jian Yang. Desnet: Decomposed scale-consistent network for unsupervised depth completion. In *Proceedings of the AAAI conference on artificial intelligence*, pages 3109–3117, 2023. 7
- [68] Zhiqiang Yan, Yuankai Lin, Kun Wang, Yupeng Zheng, Yufei Wang, Zhenyu Zhang, Jun Li, and Jian Yang. Tri-perspective view decomposition for geometry-aware depth completion. In *Proceedings of the IEEE/CVF Conference on Computer Vision and Pattern Recognition*, pages 4874–4884, 2024. 3, 2
- [69] Lihe Yang, Bingyi Kang, Zilong Huang, Xiaogang Xu, Jiashi Feng, and Hengshuang Zhao. Depth anything: Unleashing the power of large-scale unlabeled data. In *Proceedings of the IEEE/CVF Conference on Computer Vision and Pattern Recognition*, pages 10371–10381, 2024. 2, 3, 5, 6, 8
- [70] Lihe Yang, Bingyi Kang, Zilong Huang, Zhen Zhao, Xiaogang Xu, Jiashi Feng, and Hengshuang Zhao. Depth anything v2. *Advances in Neural Information Processing Systems*, 37:21875–21911, 2024. 2
- [71] Yao Yao, Zixin Luo, Shiwei Li, Jingyang Zhang, Yufan Ren, Lei Zhou, Tian Fang, and Long Quan. Blendedmvs: A large-scale dataset for generalized multi-view stereo networks. In *Proceedings of the IEEE/CVF conference on computer vision and pattern recognition*, pages 1790–1799, 2020. 5
- [72] Wei Yin, Yifan Liu, and Chunhua Shen. Virtual normal: Enforcing geometric constraints for accurate and robust depth

- prediction. *IEEE Transactions on Pattern Analysis and Machine Intelligence*, 44(10):7282–7295, 2021. [2](#), [4](#), [5](#)
- [73] Wei Yin, Chi Zhang, Hao Chen, Zhipeng Cai, Gang Yu, Kaixuan Wang, Xiaozhi Chen, and Chunhua Shen. Metric3d: Towards zero-shot metric 3d prediction from a single image. In *Proceedings of the IEEE/CVF International Conference on Computer Vision*, pages 9043–9053, 2023. [3](#)
  - [74] Weihao Yuan, Xiaodong Gu, Zuozhuo Dai, Siyu Zhu, and Ping Tan. Neural window fully-connected crfs for monocular depth estimation. In *Proceedings of the IEEE/CVF conference on computer vision and pattern recognition*, pages 3916–3925, 2022. [3](#)
  - [75] Bowen Zhang, Yidong Wang, Wenxin Hou, Hao Wu, Jindong Wang, Manabu Okumura, and Takahiro Shinozaki. Flexmatch: Boosting semi-supervised learning with curriculum pseudo labeling. *Advances in Neural Information Processing Systems*, 34:18408–18419, 2021. [3](#)
  - [76] Chongzhen Zhang, Yang Tang, Chaoqiang Zhao, Qiyu Sun, Zhencheng Ye, and Jürgen Kurths. Multitask gans for semantic segmentation and depth completion with cycle consistency. *IEEE Transactions on Neural Networks and Learning Systems*, 32(12):5404–5415, 2021. [3](#)
  - [77] Yinda Zhang and Thomas Funkhouser. Deep depth completion of a single rgb-d image. In *Proceedings of the IEEE conference on computer vision and pattern recognition*, pages 175–185, 2018. [3](#)
  - [78] Youmin Zhang, Xianda Guo, Matteo Poggi, Zheng Zhu, Guan Huang, and Stefano Mattoccia. Completionformer: Depth completion with convolutions and vision transformers. In *Proceedings of the IEEE/CVF Conference on Computer Vision and Pattern Recognition*, pages 18527–18536, 2023. [3](#), [6](#), [7](#), [1](#)
  - [79] Wending Zhou, Xu Yan, Yinghong Liao, Yuankai Lin, Jin Huang, Gangming Zhao, Shuguang Cui, and Zhen Li. Bev@dc: Bird’s-eye view assisted training for depth completion. In *Proceedings of the IEEE/CVF Conference on Computer Vision and Pattern Recognition*, pages 9233–9242, 2023. [3](#), [2](#)
  - [80] Zhi-Hua Zhou and Ming Li. Semi-supervised learning by disagreement. *Knowledge and Information Systems*, 24:415–439, 2010. [3](#)
  - [81] Yiming Zuo and Jia Deng. Ogni-dc: Robust depth completion with optimization-guided neural iterations. In *European Conference on Computer Vision*, pages 78–95. Springer, 2024. [1](#)
  - [82] Yiming Zuo, Willow Yang, Zeyu Ma, and Jia Deng. Omni-dc: Highly robust depth completion with multiresolution depth integration. *arXiv preprint arXiv:2411.19278*, 2024. [2](#), [3](#), [4](#), [6](#), [7](#), [1](#)



# PacGDC: Label-Efficient Generalizable Depth Completion with Projection Ambiguity and Consistency

## Supplementary Material

### 6. More Implementation Details

**Training Details.** *Zero-shot Depth Completion:* The training data simply concentrate all available training datasets following [50, 51], without any explicit balancing strategies as in [82]. Due to resource constraints, the training resolution is set to  $320 \times 320$ , though higher resolutions could further enhance performance, as observed in image analysis tasks [24, 59].

Due to the challenges posed by our highly diverse data setting, we modify the  $2 \times 2$  convolutions in the up/downsampling layers of SPNet to  $3 \times 3$  convolutions, as odd-sized kernels generally provide better stability [60]. This modification results in a slight increase in computational cost, as shown in Tab. 8. Notably, “Ours-T” even outperforms “SPNet-L” while requiring half the inference time and only 17% of the parameters.

Additionally, we impose a constraint that the minimum number of sparse depth pixels during training is two. This allows us to simplify the absolute term in the G2-MonoDepth loss [50] to L1 loss. The updated loss function  $\mathbb{L}$ , which measures the discrepancy between predictions  $\tilde{d}$  and our pseudo depth labels  $\hat{d}$ , is expressed as follows:

$$\begin{aligned} \mathbb{L}(\tilde{d}, \hat{d}) = & \frac{1}{\eta} \sum_{i=1}^{\eta} |T(\tilde{d}_i) - T(\hat{d}_i)| + \frac{1}{\eta} \sum_{i=1}^{\eta} |\tilde{d}_i - \hat{d}_i| \\ & + \frac{0.5}{\eta} \sum_{r=0}^3 \sum_{i=1}^{\eta} |\nabla(\rho_r(T(\tilde{d}_i) - T(\hat{d}_i)))|, \end{aligned} \quad (4)$$

where  $T$  is the standardize operation with mean deviation in [50]. The function  $\rho_r$  is the nearest neighbor interpolation at the  $1/2^r$  resolution.  $\nabla$  is the Sobel gradient in height and width directions.  $\eta$  denotes the number of valid pixels in dense labels.

**Few-shot Depth Completion:** In our few-shot experiments, we do not employ additional refinement strategies, such as SPN-like modules [7, 29, 45, 54] or depth enhancement methods [48, 49]. This ensures that our model retains SPNet’s efficiency. The training resolution is set to a randomly cropped  $256 \times 1216$ . The loss function is updated to the commonly used L1+L2 loss, following the standard practice in most intra-domain learning methods [54, 55, 78].

**Testing Details.** The details of the test datasets are provided in Tab. 7. For the uniform sampling experiment, test images are resized to a height of 320 pixels. In the sensor-captured experiment, the VOID and KITTI datasets follow standard protocols, with VOID maintaining its original resolution of

Datasets	Indoor	Outdoor	Label	Size
ETH3D [40]	✓	✓	Laser	454
Ibims [20]	✓		Laser	100
NYUv2 [42]	✓		RGB-D	654
DIODE [46]	✓	✓	Laser	771
Sintel [3]	✓	✓	Synthetic	1064
KITTI [11]		✓	Stereo	1000
VOID [58]	✓	✓	RGB-D	800

Table 7. The details of test datasets.

Method	Speed↑ (Image/s)	Param.↓ (M)	Memo.↓ (MB)	RMSE↓ (mm)	MAE↓ (mm)
SPNet-T	<b>126.6</b>	<b>35.0</b>	330	2342	857
Ours-T	121.8	39.7	<b>242</b>	<b>2143</b>	792
SPNet-L	<b>60.2</b>	<b>235.5</b>	<b>1176</b>	2271	791
Ours-L	58.7	254.4	1246	<b>1966</b>	<b>731</b>

Table 8. The inference costs under “Tiny” (T) and “Large” (L) configurations, including speed, parameters, and memory usage. Notably, the results of “Ours-T” are copied from the ablation study only using 25% training data (in gray).

480×640 and KITTI using a bottom center-cropped resolution of  $256 \times 1216$ . The final results on KITTI are obtained by averaging predictions from both original and horizontally flipped inputs following implementations in [54, 55].

### 7. More Quantitative Results

**Zero-shot Depth Completion on DDAD Dataset.** We further evaluate PacGDC on the DDAD [12] dataset, comparing to more generalizable and supervised baselines, following the standard protocol of VPP4DC [1]. The baseline results are directly taken from relevant papers. As shown in Tab. 9, the results further validate the effectiveness of PacGDC for zero-shot generalization.

Method	RMSE ↓	MAE ↓	Method	RMSE ↓	MAE ↓
BP-Net [45]	8903	2712	Marigold-DC [47]	6449	2364
VPP4DC [1]	10247	2290	DMD <sup>3</sup> C [23]	6609	1842
OGNI-DC [81]	6876	1867	<b>Ours</b>	<b>5918</b>	<b>1140</b>

Table 9. **Zero-shot depth completion** on DDAD dataset under VPP4DC protocol.

**Few-shot Comparison with Other Baselines.** We supplement Tab. 4 with additional few-shot baselines. The base-

line results on KITTI validation set are directly taken from their original papers. As shown in Tab. 10, the results further demonstrate the superiority of our model in few-shot depth completion.

Method	Shot	$RMSE \downarrow$	$MAE \downarrow$	$iRMSE \downarrow$	$iMAE \downarrow$
DepthPrompt [32]	100	1798	602	-	-
<b>Ours</b>	100	<b>911</b>	<b>229</b>	<b>2.54</b>	<b>0.96</b>
DDPMD [35]	11000	966	291	3.63	1.48
<b>Ours</b>	1000	<b>830</b>	<b>220</b>	<b>2.28</b>	<b>0.91</b>

Table 10. **Few-shot depth completion** on KITTI with 64 line LiDAR, supplementing Tab. 4.

**In-Domain Evaluation on the KITTI Dataset.** We further conduct standard in-domain evaluation by fine-tuning the pre-trained zero-shot PacGDC model on the entire KITTI training set (*i.e.*, 86K samples). As presented in Tab. 11, despite adopting a plain backbone without specialized components such as spatial propagation networks (SPNs), PacGDC delivers competitive performance on the KITTI validation set, comparable to recent state-of-the-art methods. Moreover, we submit the results of the fully fine-tuned model to the official KITTI test set leaderboard.

Method	Plain	$RMSE \downarrow$	$MAE \downarrow$	$iRMSE \downarrow$	$iMAE \downarrow$
BEV@DC [79]		720	<b>187</b>	<b>1.88</b>	<b>0.80</b>
TPVD [68]		<b>719</b>	187	-	-
BEV@DC [79]	✓	762	198	2.06	0.86
TPVD [68]	✓	764	<b>198</b>	-	-
UniDC [30]	✓	824	209	-	-
<b>Ours</b>	✓	<b>759</b>	203	<b>2.06</b>	<b>0.85</b>

Table 11. **In-domain evaluation** on KITTI validation set.

## 8. More Ablation Study

**Different Depth Foundation Models.** We evaluate our approach with four different depth foundation models: DepthAnything (DA) [69], DepthPro [2], DepthAnythingV2 (DAV2) [70], and DistillAnyDepth (DistillAD) [14]. As shown in Tab. 12, PacGDC consistently yields performance improvements over the baseline (without PacGDC), further validating the generality and effectiveness of our method.

It is worth noting that this experiment was newly introduced in response to reviewer feedback. Accordingly, our "Large" model continues to use DA and DepthPro, as reported in Tab. 6, rather than the combination of DA, DepthPro, and DAV2 used in Tab. 12.

## 9. More Visual Results

**Zero-Shot Depth Completion.** We further provide visual examples of zero-shot scenarios in Fig. 8, covering a range

DA [69]	DepthPro [2]	DAV2 [70]	DistillAD [14]	$RMSE \downarrow$	$MAE \downarrow$
				2484	990
✓				2277	857
✓	✓			2241	854
	✓	✓		2243	852
		✓	✓	2276	859
✓	✓	✓		<b>2232</b>	<b>848</b>
✓	✓	✓	✓	2279	874

Table 12. **Ablation study** on different depth foundation models. Results with our data synthesis pipeline are shaded in gray.

of datasets and sparsity levels: DIODE with 1% sparsity, ETH3D with 10% sparsity, KITTI with 4-line LiDAR, and VOID with 1500 feature points derived from a VIO system. Across these scenarios, characterized by diverse scene semantics, varying scales, and different forms of depth sparsity, PacGDC consistently achieves higher accuracy in predicting metric depth maps compared to existing baselines.

**Few-Shot Depth Completion.** Visual results for few-shot scenarios are presented in Figs. 9 and 10, using models trained with 1, 10, 100, and 1000 samples. To provide a comprehensive analysis, we also separately showcase results for 8-, 16-, 32-, and 64-line LiDAR inputs under the same few-shot training settings. Leveraging the strong pre-trained weights from our synthesis pipeline, our model demonstrates significant qualitative improvements over in-domain learning baselines across all levels of supervision.

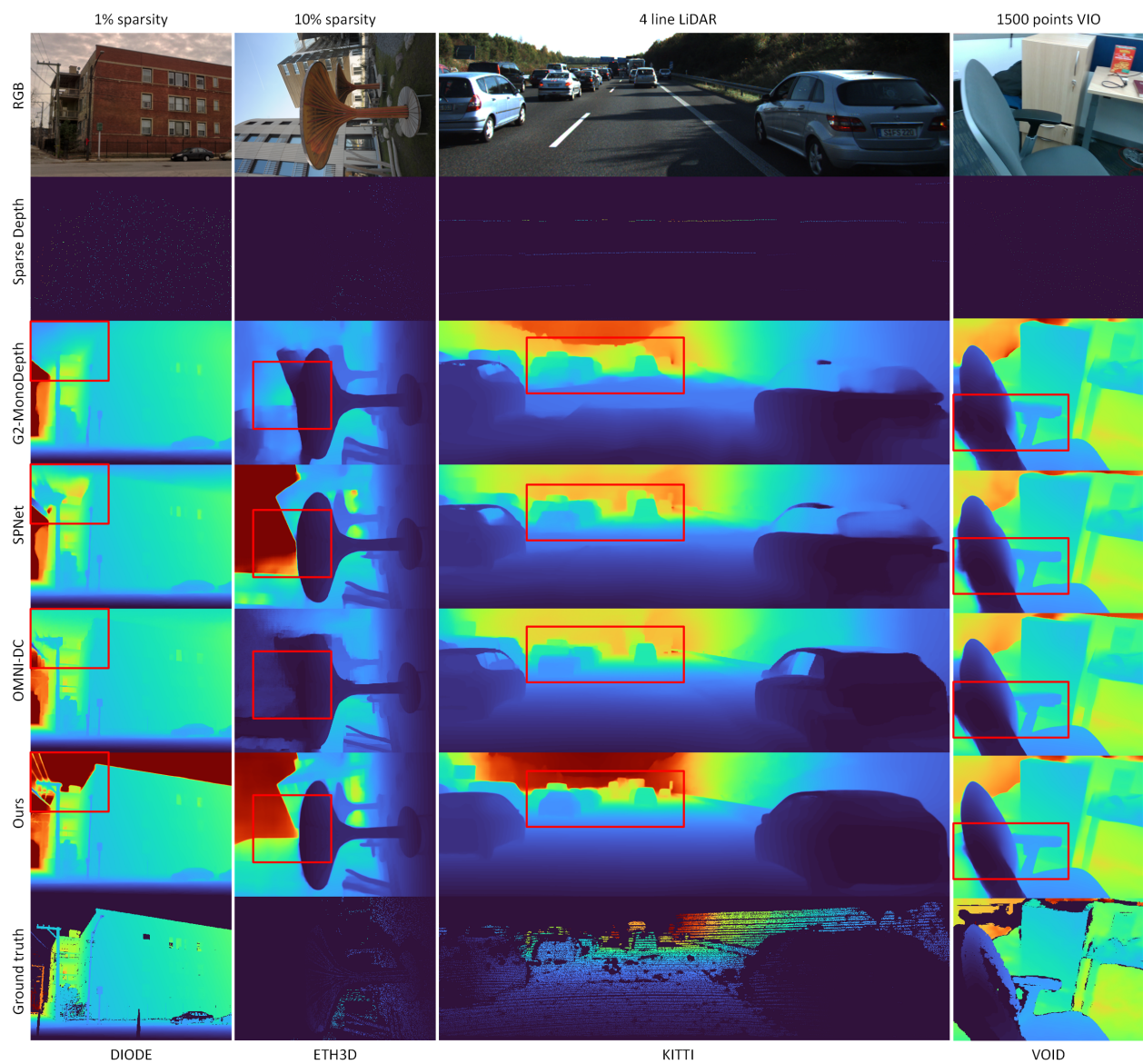


Figure 8. **Zero-shot depth completion** on unseen scenarios with different scene semantics/scales and depth sparsity/patterns.

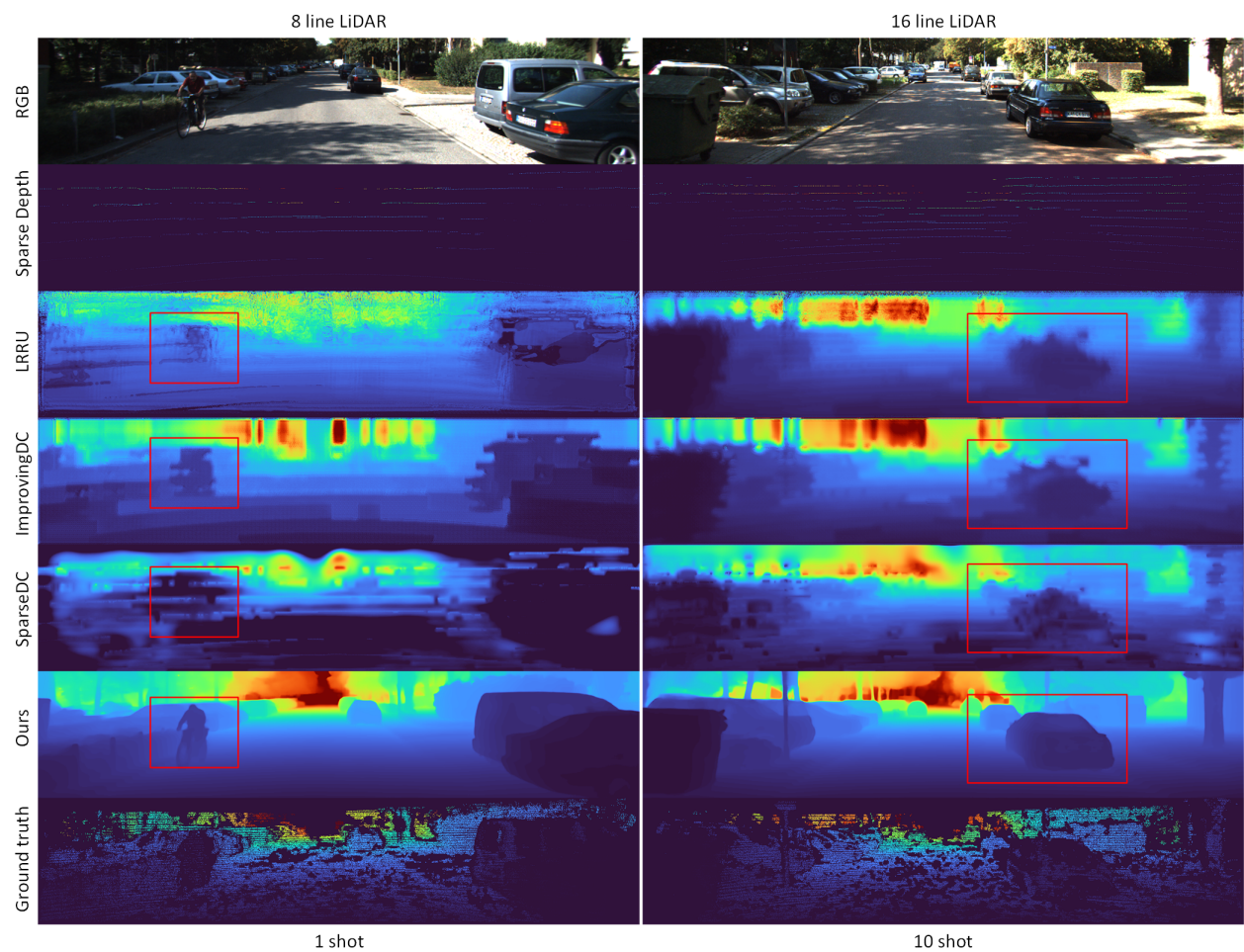


Figure 9. **Few-shot depth completion** on KITTI with 8- and 16-lines LiDAR, using models trained with 1 and 10 samples, respectively.



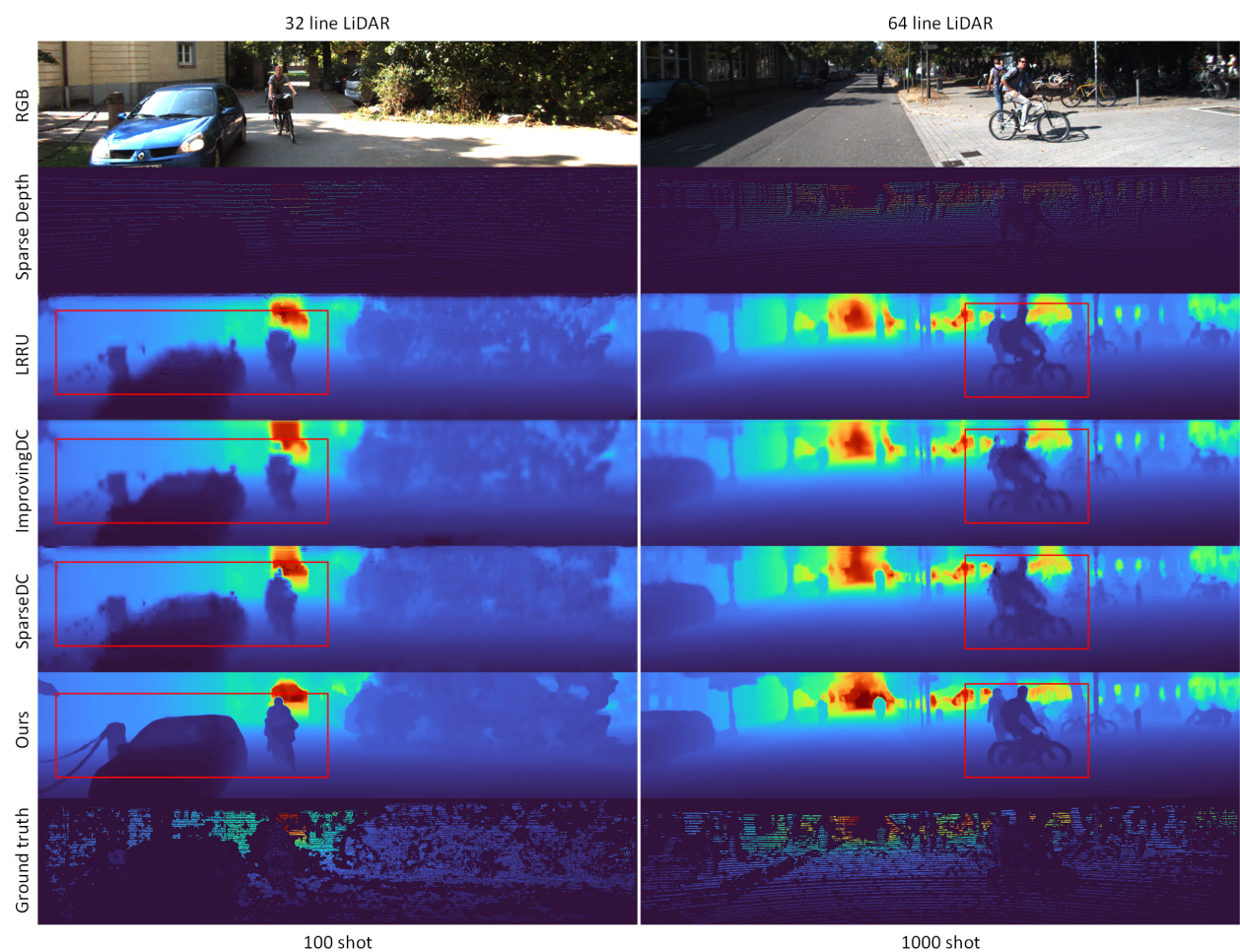


Figure 10. **Few-shot depth completion** on KITTI with 32- and 64-lines LiDAR, using models trained with 100 and 1000 samples, respectively.